Journal of Alloys and Compounds 724 (2017) 287–295

Contents lists available at ScienceDirect

Journal of Alloys and Compounds

journal homepage: http://www.elsevier.com/locate/jalcom

Shearing mechanisms of stacking fault and anti-phase-boundary forming dislocation pairs in the γ′ phase in Ni-based single crystal superalloy

Haibo Long [a], Yinong Liu [b, *], Deli Kong [a], Hua Wei [c, **], Yanhui Chen [a], Shengcheng Mao [a, ***]

[a] Beijing Key Lab of Microstructure and Property of Advanced Materials, Beijing University of Technology, 100124, Beijing, China
[b] School of Mechanical and Chemical Engineering, The University of Western Australia, Perth, WA, 6009, Australia
[c] College of Materials Science and Engineering, Nanjing Tech University, Nanjing, 211800, China

ARTICLE INFO

Article history:
Received 24 May 2017
Received in revised form
1 July 2017
Accepted 3 July 2017
Available online 4 July 2017

Keywords:
Ni-based superalloy
Anti-phase boundary
Stacking fault
Partial dislocations
Superlattice
$L1_2$ structure

ABSTRACT

Ni-based superalloys rely on high volume fractions of $L1_2$ ordered γ′ phase precipitates for strength against creep deformation at elevated temperatures. However, under certain conditions dislocations existing in the FCC γ matrix may enter the $L1_2$ γ′ phase in pairs. The shear motion of different combinations of dislocation pairs creates different planar defects in the γ′ phase, including anti-phase boundaries (APB) or stacking faults. The formation of an APB requires the shear distortion associated with an **a/2**⟨**110**⟩ dislocation and the formation of a stacking fault requires the shear distortion associated with a k⟨**112**⟩ dislocation. Given that the native dislocations in FCC structure are **a/2**⟨**110**⟩, the formation mechanism of k⟨**112**⟩ dislocations remains to be clarified. Different mechanisms have been suggested for the formation of stacking faults in the γ′ phase in the literature. In this study, the shearing motions of various partial dislocation pairs and the planar defects formed in the γ′ phase were investigated by means of transmission electron microscopy and the mechanisms were analyzed in terms of their crystallographic and energetic implications.

1. Introduction

Ni-based superalloys are commonly used for high temperature applications, e.g., typically for blades and vanes of turbine engines, because of their excellent creep resistance and high temperature strength [1–3]. Their microstructure is composed of an ordered $L1_2$-structured γ′ phase in cuboidal shapes embedded in a continuous disordered FCC γ phase matrix [4,5]. Due to its ordered structure, the γ′ phase offers much greater resistance to dislocation movement, rendering the superalloys high strength at elevated temperatures [6,7]. However, under more severe conditions, dislocations are still able to move from the γ phase matrix into the γ′ phase domains [8–10].

The Burgers vector of full dislocations in FCC γ phase is $\mathbf{b}_\gamma = \mathbf{a/2}$⟨**110**⟩, which is the full lattice vector along ⟨110⟩. For the $L1_2$ ordered γ′ phase, the full lattice vector along ⟨110⟩ is $\mathbf{b}_{\gamma'} = \mathbf{a}$⟨**110**⟩, twice in magnitude of that of the Burgers vector of the native dislocation in the γ phase. In this regard, $\mathbf{b}_{\gamma'} = \mathbf{a}$⟨**110**⟩ can be considered a "super-dislocation" of the γ′ phase and its energy state is prohibitively high, thus rarely exists in isolation. This implies that the conceptual full "super-dislocation" in the γ′ phase always exist in split partial forms, creating various types of planar defects. Fig. 1 shows the (111) plane of the $L1_2$ structure and its ABC stacking order. The native full dislocation in FCC is denoted $\mathbf{b_1}$ in the figure. The shortest lattice vector in the $L1_2$ structure along ⟨110⟩ is $\mathbf{b} = \mathbf{a}$⟨**110**⟩ (denoted **b** in the figure), which is twice as large as $\mathbf{b_1}$. This implies that a $\mathbf{b} = \mathbf{a/2}$⟨**110**⟩ dislocation moving from the γ phase into the γ′ phase only acts like a partial dislocation along ⟨110⟩ [11,12], creating an anti-phase boundary (APB) along {111} in the γ′ phase, as indicated by $\mathbf{b_1}$ in Fig. 1. It is also clear in the figure that there are three equivalent variants of APB, indicated as $\mathbf{b_1}'$ and $\mathbf{b_1}''$ in addition to $\mathbf{b_1}$. They are produced by $\mathbf{b} = \mathbf{a/2}$⟨**110**⟩ dislocations with co-planar Burgers vectors. It is also apparent that $\mathbf{b_1}' = \mathbf{b_1} + \mathbf{b_1}''$.

* Corresponding author.
** Corresponding author.
*** Corresponding author.
E-mail address: yinong.liu@uwa.edu.au (Y. Liu).

http://dx.doi.org/10.1016/j.jallcom.2017.07.020
0925-8388/

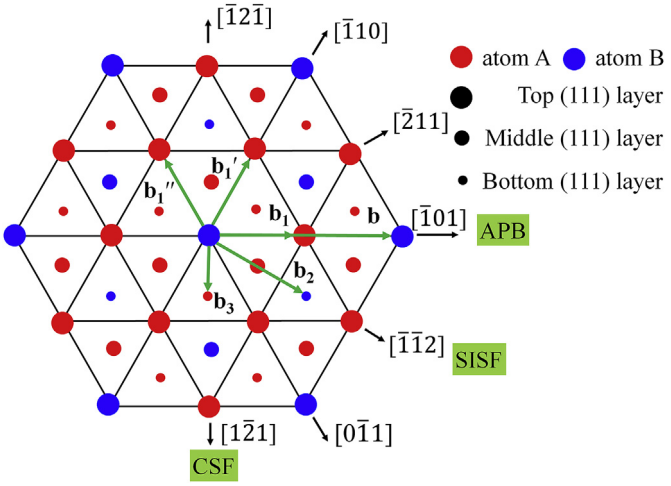

Fig. 1. Atomic structure of (111) plane and its ABC stacking ordering of $L1_2$ structure, schematically revealing the formation of different types of planar defects including anti-phase boundaries and stacking faults by the movement of partial dislocations in the γ' phase.

The creation of APB incurs an energy increase, or barrier, to the process [12,13]. To reduce this energy barrier, dislocation pairs of the same Burgers vector are required, so that the APB created by the first dislocation is negated by the second dislocation moving through [14,15]. In addition to $\mathbf{b_1} = \mathbf{a/2}\langle\mathbf{110}\rangle$ dislocation pairs and APBs, stacking faults along ⟨111⟩ directions have also been observed. A stacking fault may be created by gliding of $\mathbf{b_2} = \mathbf{a/3}\langle\mathbf{112}\rangle$ or $\mathbf{b_3} = \mathbf{a/6}\langle\mathbf{112}\rangle$ (Fig. 1) dislocations [16–18]. The gliding of a $\mathbf{b_2} = \mathbf{a/3}\langle\mathbf{112}\rangle$ partial dislocation in the γ' phase produces a superlattice intrinsic stacking fault (SISF) [19,20] and the gliding of a $\mathbf{b_3} = \mathbf{a/6}\langle\mathbf{112}\rangle$ dislocation produces a complex stacking fault (CSF) [10,21]. It is also obvious that $\mathbf{b_3} = \mathbf{b_2} \pm \mathbf{b_1}$. In this regard, CSF can be considered of a compound planar defect of SISF and APB.

The energy states of the fore-mentioned three types of planar defects, i.e., energy barriers for the gliding of the three types of partial dislocations into the γ' phase, have been estimated to follow the order of CSF > APB > SISF [22–24]. Gliding of a $\mathbf{b_3} = \mathbf{a/6}\langle\mathbf{112}\rangle$ partial dislocation, which produces CSF, has the highest energy barrier, i.e., is the most difficult. However, when a $\mathbf{b_3} = \mathbf{a/6}\langle\mathbf{112}\rangle$ partial dislocation glides behind a $\mathbf{b_2} = \mathbf{a/3}\langle\mathbf{112}\rangle$ partial dislocation, it will transform the SISF region into an APB, thereby experiences a lower energy barrier compared with CSF alone [25,26]. Such $\mathbf{b_2} + \mathbf{b_3}$ partial dislocation pairs have been observed to operate at intermediate temperatures around 750 °C [27,28]. Given that (energy barrier) APB > SISF, it can also be understood that shearing by a $\mathbf{b_1} = \mathbf{a/2}\langle\mathbf{110}\rangle$ dislocation, which produces APB, is more difficult than the shearing by a $\mathbf{b_2} = \mathbf{a/3}\langle\mathbf{112}\rangle$, which produces SISF. However, $\mathbf{b_1} = \mathbf{a/2}\langle\mathbf{110}\rangle$ dislocation pairs have been observed experimentally after creep testing at intermediate temperatures [29,30], and no clear explanation has been given in the literature.

Formation of stacking faults requires k⟨**112**⟩ partial dislocations (k is a constant expressing the magnitude of a specific dislocation), which are not native in the FCC crystal. Three different models have been proposed to explain the mechanisms for the creation of these dislocations. In the first model [30,31], the partial dislocations are created by dissociation of **a/2[011]** via $\mathbf{a}/2[011] \rightarrow \mathbf{a}/3\left[\bar{1}12\right] + \mathbf{a}/6\left[21\bar{1}\right]$. This reaction represents a free energy increase for the dislocations. Also, the Burgers vectors of the two partial dislocations created are not parallel, thus cannot explain the observation of partial dislocation pairs of like Burgers vectors [27,32]. The second model [33–35] proposed a $\mathbf{a}/2[011] \rightarrow \mathbf{a}/6\left[\bar{1}12\right] + \mathbf{a}/6[121]$ reaction. As discussed above, the APB created by the shearing of **a/2[011]** has a lower energy state than the CSF created by the shearing of either of the two **a/6⟨112⟩** partial dislocations. In this regard, the motivation (necessity) of the above dislocation decomposition appears to be unsupported. The third model [36,37] proposed **a/2[101]** + **a/2[011]** → **a/3[112]** + **a/6[112]** for the production of the ⟨112⟩ partial dislocations. This appears to be the only plausible mechanism. However, the situation where partial dislocation pairs of dislike Burgers vectors are formed is not covered in this case.

Given the obvious deficiencies and uncertainties concerning these models, we conducted this study to investigate the formation mechanisms of partial dislocation pairs and planar defects in the γ' phase in a Ni-based single crystal superalloy under the condition of mechanical straining at intermediate temperatures (creep testing). In-situ transmission electron microscopy (TEM) has been shown to be useful in observing dislocation activities during mechanical deformation [38–48]. However, the fast mobility of dislocations can still make it difficult sometimes to observe and record dislocation reactions and to determine the Burgers vectors of dislocations. Thus, ex-situ TEM study was also used in this study.

2. Experimental procedure

The chemical composition of the Ni-based single crystal alloy used is given in Table 1. The single crystal was grown by directional investment casting method, and the growth direction is [001]. The single crystal sample was heat treated following a process including solution treatment at 1275 °C for 4 h (air cooling), aging at 1100 °C for 2 h (air cooling) and a second aging at 850 °C for 24 h (air cooling). Creep testing was performed at 750 °C under a tensile stress of 750 MPa along the [001] direction. After creep test, thin disc specimens perpendicular to the [001] loading direction were cut from the creep test samples for TEM examination. TEM specimens were prepared by twin-jet electrochemical polishing in an electrolyte of 5% perchloric acid and 95% ethanol at −30 °C. TEM examination was conducted using a JEOL-2010 transmission electron microscope operating at 200 kV.

3. Results

Fig. 2 shows the creep curves of three samples tested at 750 °C under a tensile stress of 750 MPa. The testing of one sample was interrupted in the early stage of creep (stage I), the second sample in the intermediate steady state of creep (stage II), and the third sample was tested till rupture (stage III). The creep rate decreased gradually within the first ~10 h and then remained nearly unchanged up to ~1200 h before finally increased rapidly to rupture at ~1450 h.

Fig. 3 shows TEM examination of the microstructures of the three specimens, revealing defect evolution during creep. The observing direction is [001], as confirmed by the selected area electron diffraction (SAED) patterns shown in the inset in Fig. 3(a). The gray cuboidal blocks are the γ' phase, and the light continuous phase is γ. These two phases arrange coherently along ⟨100⟩ directions. A few native dislocations can be seen along the γ/γ' interfaces inside the γ phase. No dislocations were found inside the γ'

Table 1
Chemical composition of the experimental alloy (wt. %).

Co	Cr	Mo	W	Al	Ti	Ta	C	Ni
9.0	12.0	2.0	4.0	4.5	2.5	5.0	(0.01)	Bal.